



Construction of bismuth-deposited $\text{Bi}_4\text{O}_5\text{Br}_2$ complex and exploration of its photocatalytic properties

Xin Zhou¹, Chuang Liu¹, Zhi Zhang¹, Piao Chen¹, Yun Yang², and Shuijin Yang^{1,*}

¹College of Chemistry and Chemical Engineering, Hubei Key Laboratory of Pollutant Analysis & Reuse Technology, Hubei Normal University, Huangshi 435002, Hubei, China

²College of Chemistry and Environmental Engineering, Hanjiang Normal University, Shiyang 442000, Hubei, China

Received: 21 April 2022

Accepted: 28 October 2022

Published online:

16 February 2023

© The Author(s), under exclusive licence to Springer Science+Business Media, LLC, part of Springer Nature 2023

ABSTRACT

$\text{Bi}/\text{Bi}_4\text{O}_5\text{Br}_2$ composite photocatalysts with different loading were prepared by ethylene glycol reduction method. The successful construction of the composite was confirmed by X-ray diffraction, Fourier transform infrared, scanning electron microscope, photoluminescence, UV–Vis diffuse reflection spectroscopy, and X-ray photoelectron spectroscopy. The prepared $\text{Bi}/\text{Bi}_4\text{O}_5\text{Br}_2$ composite can degrade the colored dye RhB and the colorless substance BPA under simulated visible light. The catalytic activity of the composite is obviously improved compared with that of the pure substance, and the photocatalytic performance of 5% loading of composite sample is the best. Through the experiments of photoluminescence spectrum and fluorescence decay curve, it is confirmed that the photo-generated carrier separation efficiency of 5% loading of composite sample is the highest. Radical trapping experiments show that h^+ plays a major role. The improvement of photocatalytic activity of the composite is attributed to the plasmon resonance effect of Bi, which promotes the transfer and separation of semiconductor interface charge. The composite material has good cycle stability, which provides a research idea for the photocatalytic treatment of wastewater.

1 Introduction

With the increase of industrialization and the human population, a large number of drug compounds, organic pollutants such as dye and heavy metal ions was introduced into groundwater [1, 2]. Organic dyes, as an important part of water pollution is threatening the environment and human health, such

as CIP and BPA [3, 4]. Therefore, choose the appropriate methods to remove these pollutants is a very key question. Photocatalytic technology because of its good capability of oxidation and ecological friendliness was widely used in degradation of the organic pollutants [5, 6]. It was well known that the photocatalytic degradation using solar power, selective oxidation and hydrogen evolution reaction, etc.

Address correspondence to E-mail: yangshuijin@hunu.edu.cn

Therefore, to improve the utilization of solar energy, we need preparation has good response of the visible light photocatalyst [7]. Semiconductor photocatalytic technology as a reliable, green and efficient solar energy conversion and environmental purification method was more and more attention to [8].

Traditional TiO_2 catalyst has low cost, stable chemical properties and high oxidation ability [9, 10]. However, the traditional practical application of photocatalyst was quite limited, because the only response to ultraviolet light, and the visible light utilization rate was low, wide band gap and quantum effect. Bismuth-based photocatalysts had a non-toxic, strong oxidizing, narrow band gap, high stability, and visible light response properties, its photocatalytic used widely [11, 12]. Marzouqi synthesized $\text{BiOCl/g-C}_3\text{N}_4$ heterojunction by microwave-assisted method for photocatalytic degradation of amine drug nizatidine, showing good photocatalytic performance, which was attributed to the heterojunction interface promotes electron-hole pair separation [13]. Guan prepared superhydrophobic BiOBr/Ag copper mesh composites, which exhibited high photocatalytic activity and stable oil/water separation efficiency in the degradation of RhB and MB, which could be attributed to the wide range of light absorption range widening and reduction of the band gap [14]. Deng synthesized $\text{BiOCl/Bi/Bi}_2\text{O}_3/\text{rGO}$ heterojunctions with oxygen vacancies by in situ reduction, which could completely degrade 2-nitrophenol, which was attributed to the synergy of oxygen vacancies, heterojunctions and metallic Bi effect [15]. Zeng C/ BiOI composite material was synthesized, showed higher activity of photocatalytic degradation of MO and stable performance of nitrogen fixation [16]. Half metal bismuth (Bi) since it had the surface plasma resonance (SPR) and cocatalyst purposes, aroused the interest of the researchers widely [17, 18].

Among the bismuth-rich oxyhalide materials, $\text{Bi}_4\text{O}_5\text{Br}_2$ had high chemical stability, large surface area, unique electronic structure and high light absorption ability [19]. However, $\text{Bi}_4\text{O}_5\text{Br}_2$ materials have the disadvantages of narrow visible light absorption range (below 450 nm), low redox potential and high charge carrier recombination rate [20–22]. To overcome these shortcomings, many approaches had been employed, including the introduction of active centers [23], the synthesis of hybrids [24], control of crystal surfaces, and morphology engineering [25].

For example, the deposition of noble metals into $\text{Bi}_4\text{O}_5\text{Br}_2$ had been demonstrated to be an effective and facile strategy to optimize the catalytic performance of this material [26]. By adjusting the deposition content, the electronic structure, light absorption capacity, number of active centers, and electron-hole pair separation rate of the catalyst can be adjusted [27]. Therefore, we tried to deposit semi-metal Bi on $\text{Bi}_4\text{O}_5\text{Br}_2$, using the SPR effect of Bi to promote the separation of charge carriers and improve the photocatalytic performance of the catalyst monomer.

This article used ethylene glycol as the reducing agent and the method of reduction in situ deposition on the $\text{Bi}_4\text{O}_5\text{Br}_2$ microspheres Bi elemental nanoparticles. $\text{Bi/Bi}_4\text{O}_5\text{Br}_2$ composites with different percentages were prepared by controlling the content of $\text{Bi}(\text{NO}_3)_3 \cdot 5\text{H}_2\text{O}$. The $\text{Bi/Bi}_4\text{O}_5\text{Br}_2$ composites were analyzed by a series of characterizations such as XRD, SEM, TEM, FT-IR and PL. And simulation for degradation of RhB and BPA, visible light photocatalytic activity is higher than the pure $\text{Bi}_4\text{O}_5\text{Br}_2$ composite material after. The activity of ascension can be attributed to due to the existence of the SPR effect, metal Bi as electron traps to promote light stimulates the carrier separation and interfacial charge transfer. In addition, reaction of $\cdot\text{O}_2^-$, $\cdot\text{OH}$ and h^+ kinds of active species and the possible photocatalytic mechanism was studied, further verify the theory.

2 Materials and method

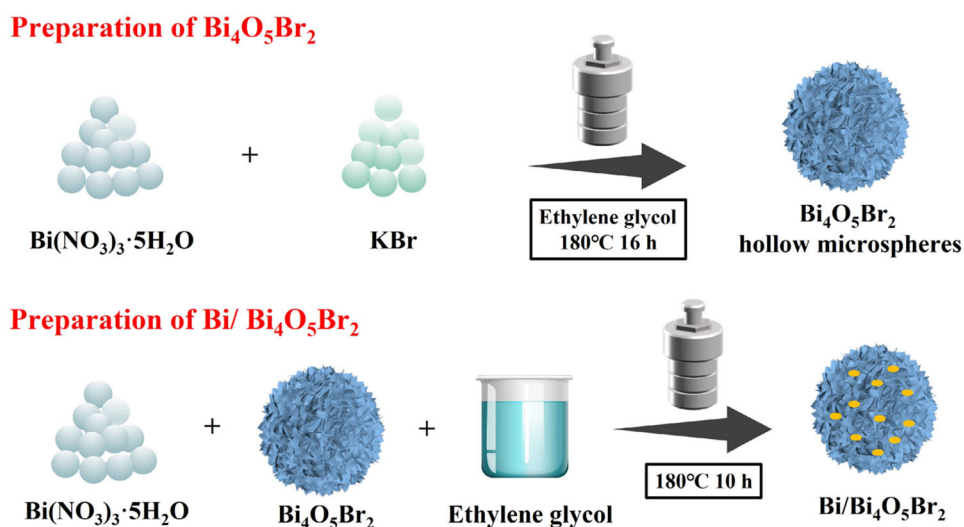
2.1 Materials

All chemical reagents used in this experiment were of analytical grade, RhB and NOR were purchased from Aladdin, and other reagents were purchased from Sinopharm Chemical Reagent Co. Ltd.

2.2 Catalyst preparation

Through the synthesis $\text{Bi}_4\text{O}_5\text{Br}_2$ solvent hot method, specific steps are as follows (Scheme 1): Firstly, 0.3638 g bismuth nitrate pentahydrate was dissolved in 5 mL ethylene glycol and stirred for 15 min. In the second step, 0.0595 g KBr was dissolved in 15 mL ethanol and stirred for 30 min. Then, the second step slowly add the solution to the first step in the solution. Stir for 1 h, and transfer to a 45 mL reaction kettle. Then in 180 °C, reaction 16 h after natural

Scheme 1 Schematic diagram of the preparation method of $\text{Bi}_4\text{O}_5\text{Br}_2$ and $\text{Bi}/\text{Bi}_4\text{O}_5\text{Br}_2$



cooling, water and ethanol washing three times, respectively under 60 °C get $\text{Bi}_4\text{O}_5\text{Br}_2$ sample after drying.

The preparation of photocatalyst $\text{Bi}/\text{Bi}_4\text{O}_5\text{Br}_2$ as follows (Scheme 1): 0.092 g bismuth nitrate pentahydrate was dissolved in 40 mL ethylene glycol, and after stirring for 30 min, a certain amount of $\text{Bi}_4\text{O}_5\text{Br}_2$ was added respectively. Stir in 1 h after move to 45 mL in the reaction kettle, maintain 10 h under 180 °C, after natural cooling, water and ethanol washing three times, respectively under 60 °C get the samples of $\text{Bi}/\text{Bi}_4\text{O}_5\text{Br}_2$ composite after drying. With Bismuth nitrate pentahydrate as bismuth source, when the loading is 0%, 2%, 5% and 10%, the samples are recorded as $\text{Bi}_4\text{O}_5\text{Br}_2$, BOB-2, BOB-5 and BOB-10, respectively.

2.3 Characterization

X-ray powder diffraction was tested by an X-ray diffractometer (X'Pert PRO MPD) with a working voltage of 40 kV and a working current of 200 mA. In order to analyze the crystal phase structure and crystallinity of the material. The microscopic morphologies of the catalysts were analyzed by scanning electron microscopy (SEM, Gemini 300, 20 kV) and transmission electron microscopy (TEM, FEI Talos F200S, USA, 200 kV), using X-ray photoelectron spectroscopy (XPS, ESCALAB 250XL) and energy dispersive spectrometers (EDS, oxford x-max 80 T) to study the elements and valences contained in the catalyst. Infrared spectroscopy (FT-IR) was acquired using a Fourier transform infrared spectrometer

(Perkin Elmer Spectrum RX I). At the same time, using BaSO_4 as the reference background, a spectrophotometer (UV2600, Japan) was used to obtain the ultraviolet–visible diffuse reflectance spectrum (UV–Vis DRS). The nitrogen adsorption–desorption curves of the catalysts were determined by a specific surface area analyzer (ASAP 2460). The fluorescence spectra (PL) of the samples were obtained on an F-4700 spectrophotometer with the excitation wavelength set to 250 nm.

3 Results and discussion

3.1 Crystal structure analysis

The crystal phase structure and purity of the samples were analyzed using X-ray powder diffraction in Fig. 1. The results show that for $\text{Bi}/\text{Bi}_4\text{O}_5\text{Br}_2$, all diffraction peaks are highly matched with the orthorhombic PDF card No. 37-0699. The characteristic peaks of the synthesized samples are at $2\theta = 29.4, 31.68, 32.0$ and 45.4° , corresponding to the (113), (402), (020) and (422) crystal planes, respectively. $\text{Bi}_4\text{O}_5\text{Br}_2$ has characteristic diffraction peaks of elemental Bi. When the loading is 2%, BOB-2, BOB-5 and BOB-10 have characteristic diffraction peaks of elemental Bi. And we can see that when the loading is larger, there are more characteristic diffraction peaks of Bi, and the intensity of the peaks is also larger. Through XRD analysis, it can be preliminarily seen that the sample has no other diffraction peaks, and the peak shape is sharp. This shows that the synthetic

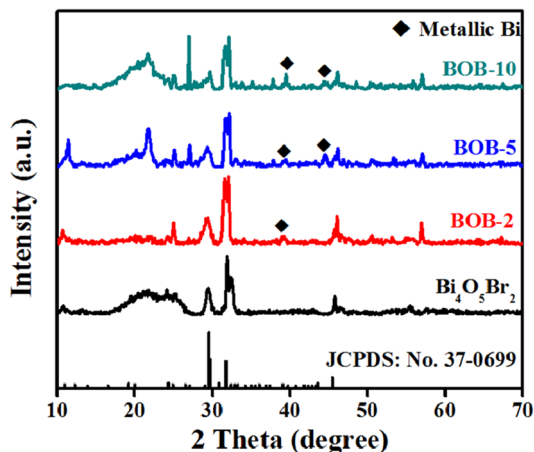


Fig. 1 XRD patterns of $\text{Bi}_4\text{O}_5\text{Br}_2$, BOB-2, BOB-5 and BOB-10

material is of high purity and good crystallinity. There is a packet peak in the Fig. 1. The possible reason is that the sample in the sample tank is not uniformly dispersed, and the sample tank has a peak.

As shown in Fig. 2, the chemical bond properties and functional groups of $\text{Bi}_4\text{O}_5\text{Br}_2$ and Bi/ $\text{Bi}_4\text{O}_5\text{Br}_2$ composites were analyzed by infrared spectroscopy. It can be seen from the figure that there is infrared absorption at the wave number 546 cm^{-1} , which is the Bi-O signal [24]. There is infrared absorption at 1062 cm^{-1} , which belongs to Bi-Br signal [28]. Compared with $\text{Bi}_4\text{O}_5\text{Br}_2$, we can see that the infrared absorption peak of the complex has a certain deviation, which may be caused by the introduction of elemental Bi.

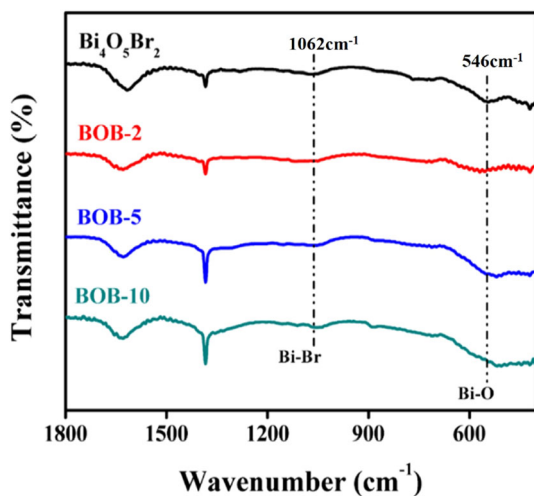


Fig. 2 FT-IR of $\text{Bi}_4\text{O}_5\text{Br}_2$, BOB-2, BOB-5 and BOB-10

3.2 Composition and chemical state analysis

The element composition and chemical valence state of BOB-5 composite material were analyzed by XPS characterization. It can be seen from Fig. 3a that the XPS measurement full spectrum shows that the synthesized sample contains C (reference element), Bi, O, and Br. Figure 3b-d further provide high-resolution XPS spectra of Bi, Br, and O. In Fig. 3b, the appearance of two strong peaks at 159.11 and 164.31 eV is attributable to the Bi^{3+} structure of Bi 4f7/2 and Bi 4f5/2. The small peaks at 156.83 and 162.12 eV belong to the signal of elemental Bi. It can be seen in Fig. 3c that two peaks appear at the binding energies of 68.22 and 69.31 eV, indicating the existence of Br^{5+} structures in the BOB-5 composite sample. The O 1s energy spectrum can be divided into two peaks, where the peak at 529.71 eV corresponds to the lattice oxygen in the material, and the peak at 531.50 eV corresponds to the surface hydroxyl groups and water molecules adsorbed on the composite material.

3.3 Micro-topography analysis

As shown in Fig. 4, the microstructure of the catalyst was analyzed by scanning electron microscopy. From Fig. 4a, b, the morphology of $\text{Bi}_4\text{O}_5\text{Br}_2$ is a wool ball structure stacked by nanosheets, and the size is about 2–4 μm . From Fig. 4c, d, we can see that the BOB-5 composite prepared by the hydrothermal method presents self-assembled flower-like microspheres with an average size of about 5 μm . Compared with pure $\text{Bi}_4\text{O}_5\text{Br}_2$, the volume of the BOB-5 sample is increased, which can be attributed to the introduction of semi-metallic Bi. Compared with the pure substance, the morphology of the composite still maintains the microsphere structure. This can also show that Bi doping has no obvious effect on the surface morphology of $\text{Bi}_4\text{O}_5\text{Br}_2$, and this scheme is feasible.

Further microstructural analysis was performed by transmission electron microscopy (TEM) in Fig. 5a. It can be observed from the TEM image that the edge of the BOB-5 sample exhibits irregular geometric shapes, and nanoparticles are attached to the surface. The edge regions of individual nanosheets were analyzed by high-resolution transmission electron microscopy (HRTEM) in Fig. 5b. The results show that BOB-5 exhibits continuous and clear lattice fringes with an average spacing of 0.328 nm and

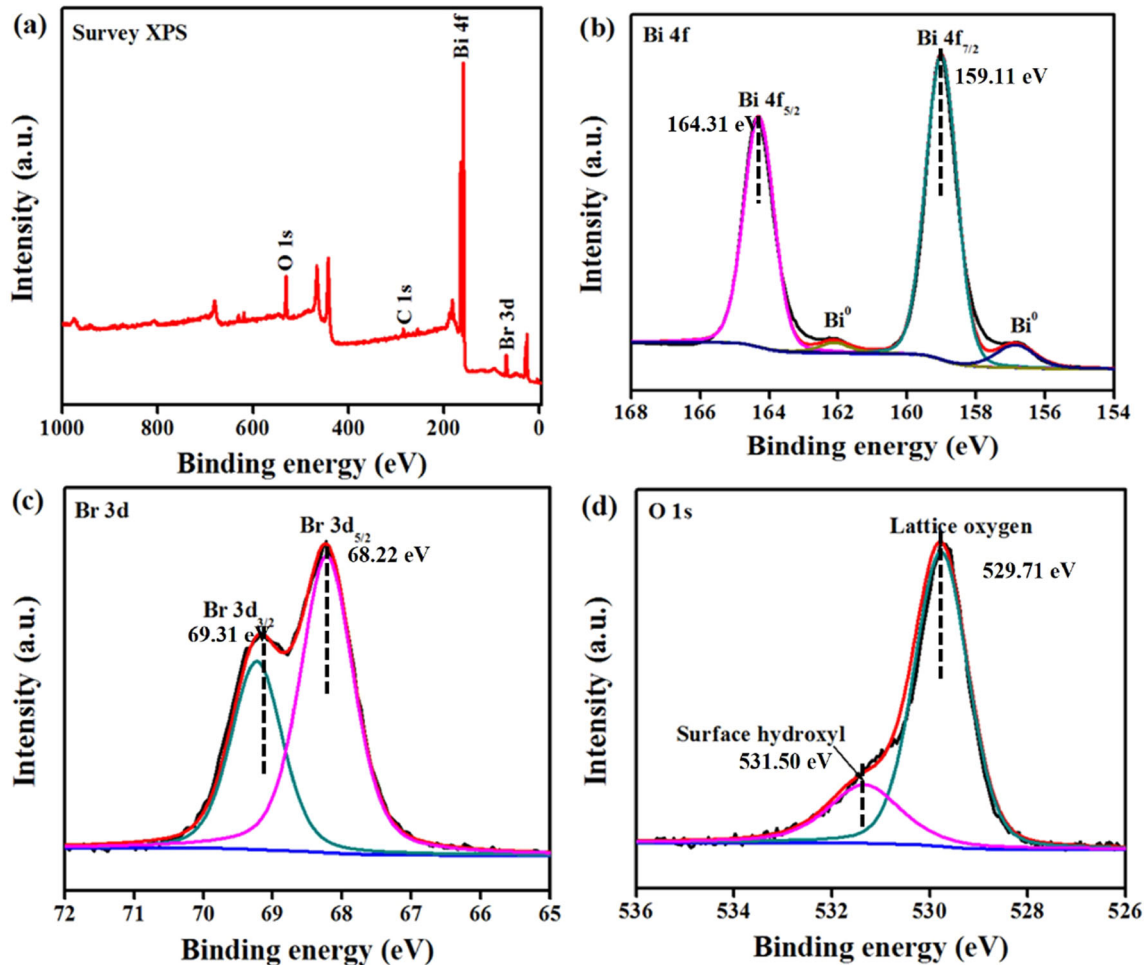


Fig. 3 The full spectrum of the XPS sample of BOB-5 (a); the high-resolution XPS spectrum of Bi 4f (b), Br 3d (c) and O 1 s (d)

0.940 nm, which correspond to the metallic Bi (012) and $\text{Bi}_4\text{O}_5\text{Br}_2$ (10–1) crystal planes, respectively.

The HAADF-STEM image of the BOB-5 complex, the corresponding element distribution image spectrum, and the EDS energy spectrum are shown in Fig. 6. It can be concluded that BOB-5 contains three elements, Bi, Br and O, and the element distribution is relatively uniform. No other impurity elements exist.

3.4 Photocatalytic performance and stability analysis

In order to further study the photocatalytic activity of Bi/ $\text{Bi}_4\text{O}_5\text{Br}_2$ complexes, the colored dye RhB and the colorless substance BPA were selected as simulated pollutants for photocatalytic degradation. As shown in Fig. 7a, c, $\text{Bi}_4\text{O}_5\text{Br}_2$, BOB-2, BOB-5 and BOB-10 were selected for RhB and BPA photocatalytic

degradation experiments. The UV–Vis absorption spectrum (Fig. 7a) shows that both the pure substance and the composite material have good degradation effect, and the degradation effect of the composite material is higher than that of $\text{Bi}_4\text{O}_5\text{Br}_2$. Among them, BOB-5 has the best degradability. Under the action of visible light, 50 mL of 10 mg/L RhB can be degraded completely within 40 min, while the degradation rate of pure $\text{Bi}_4\text{O}_5\text{Br}_2$ is only about 56%. For the colorless substance BPA (Fig. 7c), the degradation effect of pure substance is not very good. Under the action of visible light, the degradation rate of BPA (50 ml 10 mg/L) within 120 min is only about 20%. The degradation effect of the composite material is obviously improved. The degradation rate of BOB-5 can reach more than 90% in 120 min, and the degradation ability is the best. This indicates that Bi/ $\text{Bi}_4\text{O}_5\text{Br}_2$ composites prepared with $\text{Bi}(\text{NO}_3)_3 \cdot 5\text{H}_2\text{O}$ as Bi source have good photocatalytic

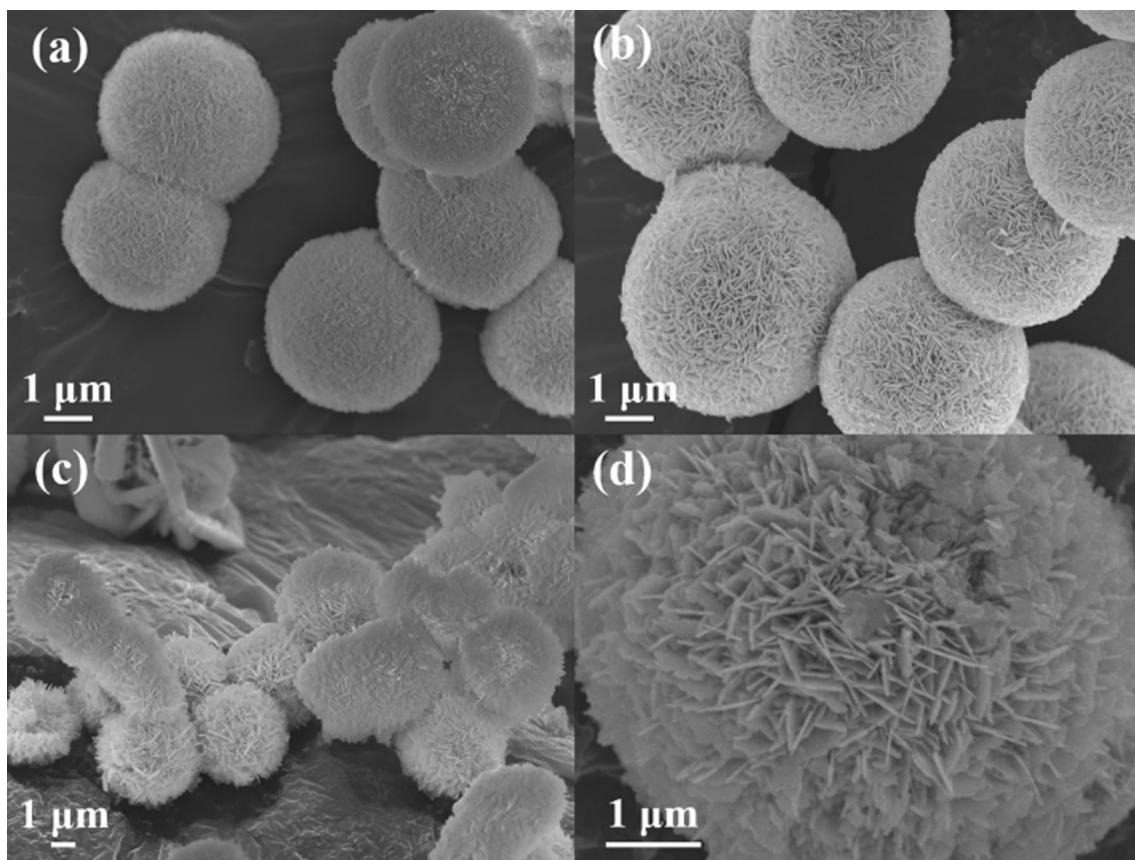


Fig. 4 a-b $\text{Bi}_4\text{O}_5\text{Br}_2$; c-d SEM images of BOB-5 samples

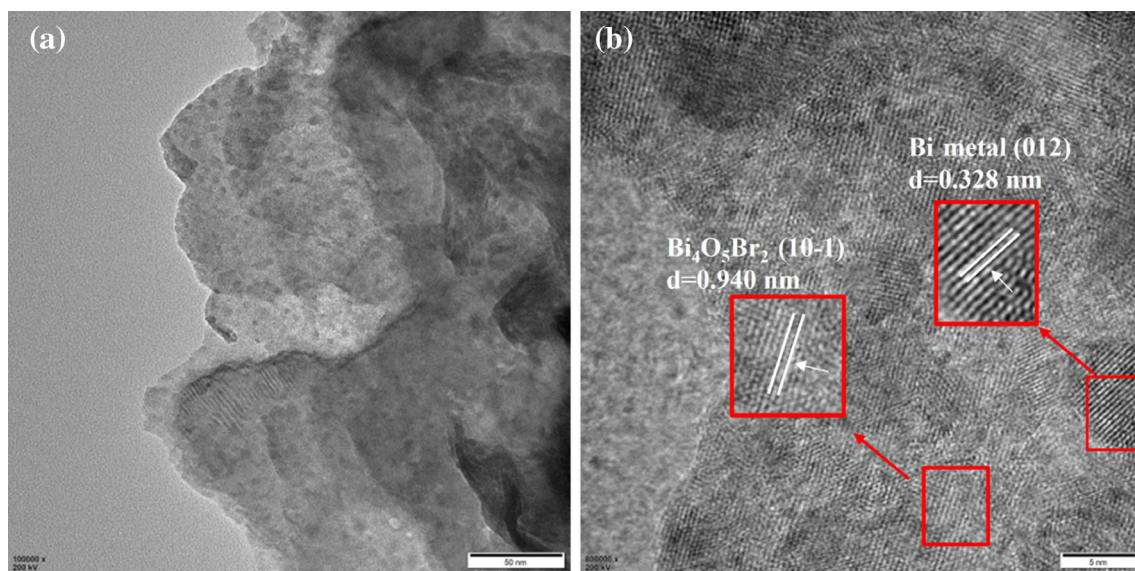
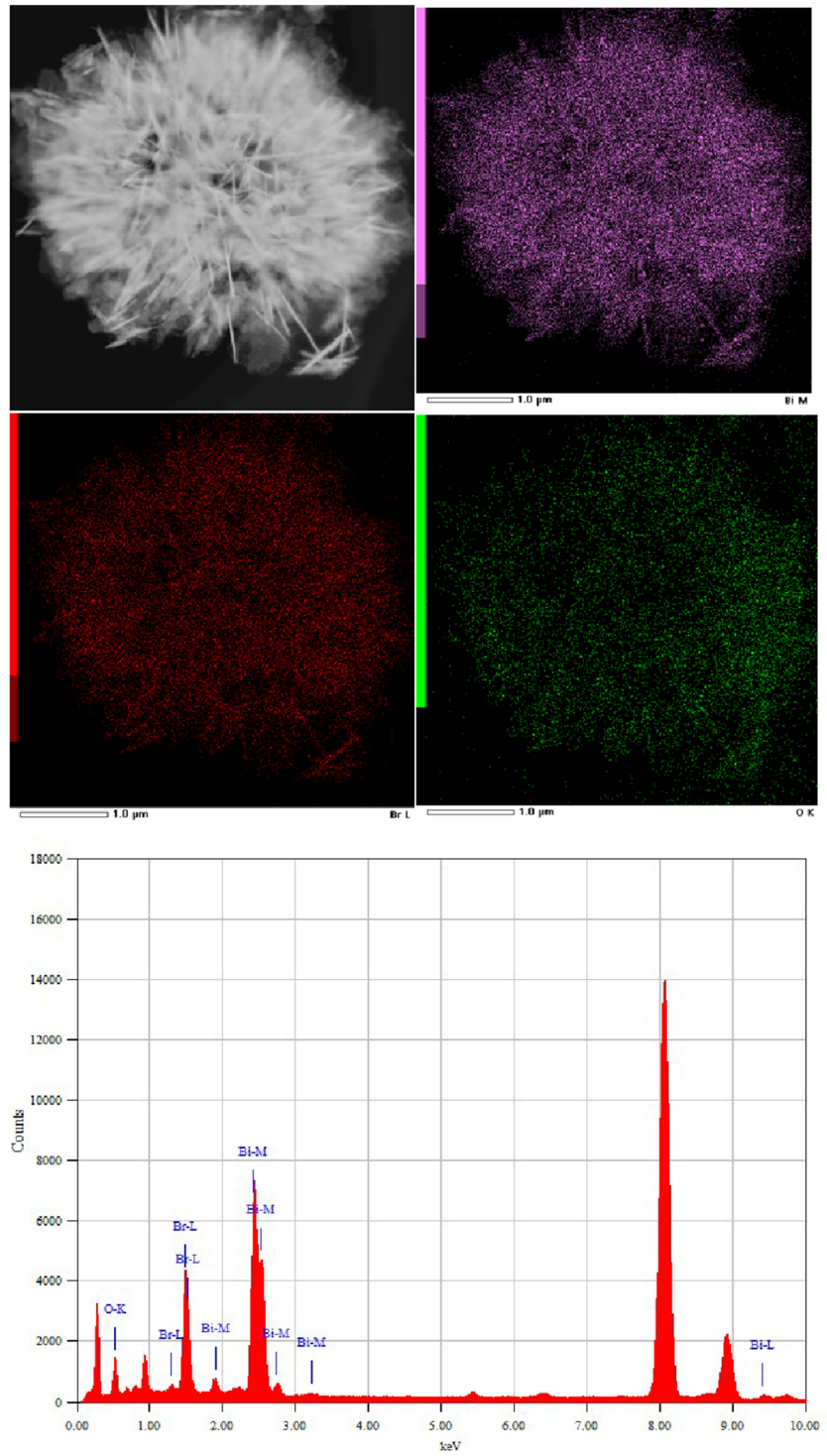


Fig. 5 TEM image (a) and HRTEM image (b) of BOB-5

performance. Figure 7b and Fig. 7d are the simulated kinetic models for the degradation of RhB and BPA, respectively. Regardless of which pollutant is

degraded, we can clearly find that the degradation rate of the complex is faster than that of the pure substance. Among them, BOB-5 has the fastest

Fig. 6 HAADF-STEM image of BOB-5 and the corresponding element distribution image spectrum and EDS energy spectrum



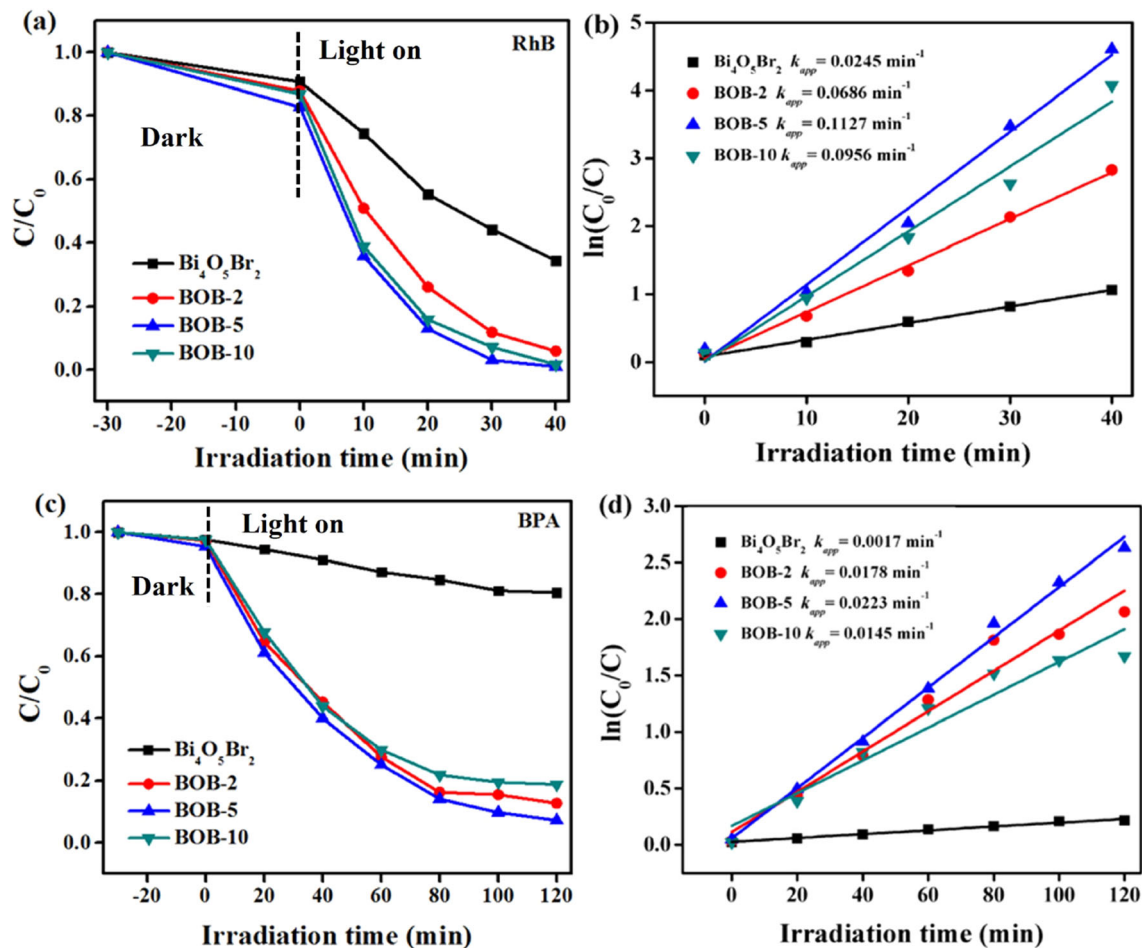


Fig. 7 a-b UV-Vis absorption spectra and pseudokinetic models of RhB degradation by $\text{Bi}_4\text{O}_5\text{Br}_2$, BOB-2, BOB-5 and BOB-10; c-d UV-Vis absorption spectra and pseudokinetic models of BPA degradation by $\text{Bi}_4\text{O}_5\text{Br}_2$, BOB-2, BOB-5 and BOB-10

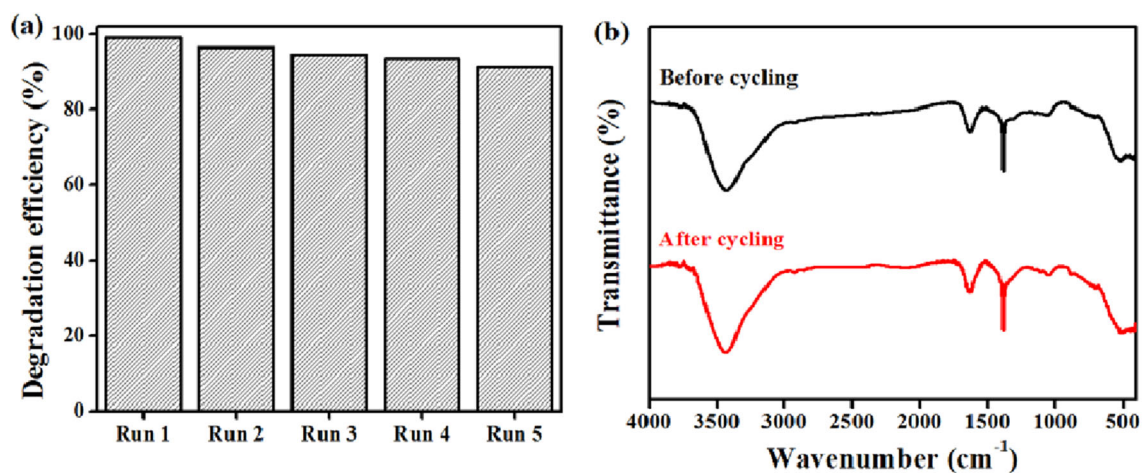


Fig. 8 Five cycle experiments of RhB degradation by BOB-5 under visible light (a); FT-IR spectra of BOB-5 after cycling experiments (b)

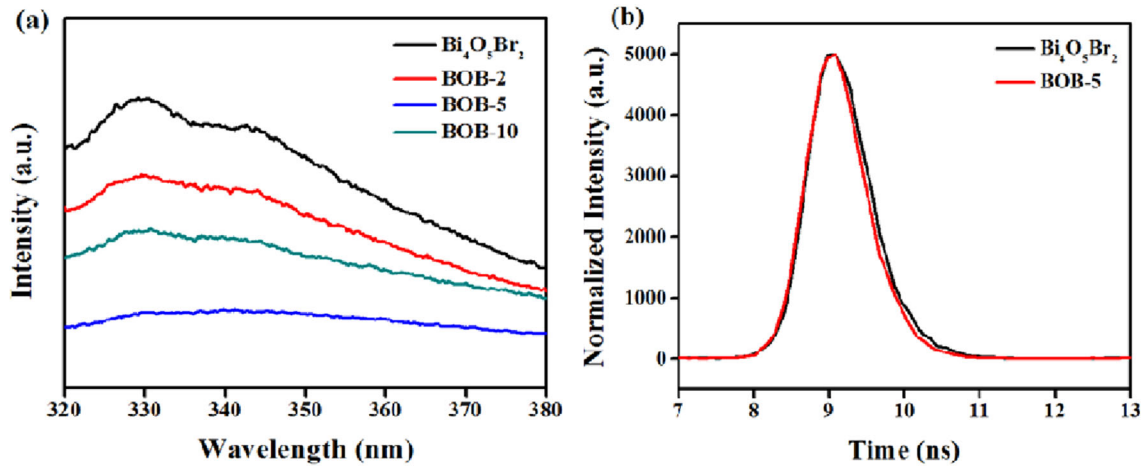


Fig. 9 Fluorescence spectra of $\text{Bi}_4\text{O}_5\text{Br}_2$, BOB-2, BOB-5 and BOB-10(a); Fluorescence decay curves of $\text{Bi}_4\text{O}_5\text{Br}_2$ and BOB-5(b)

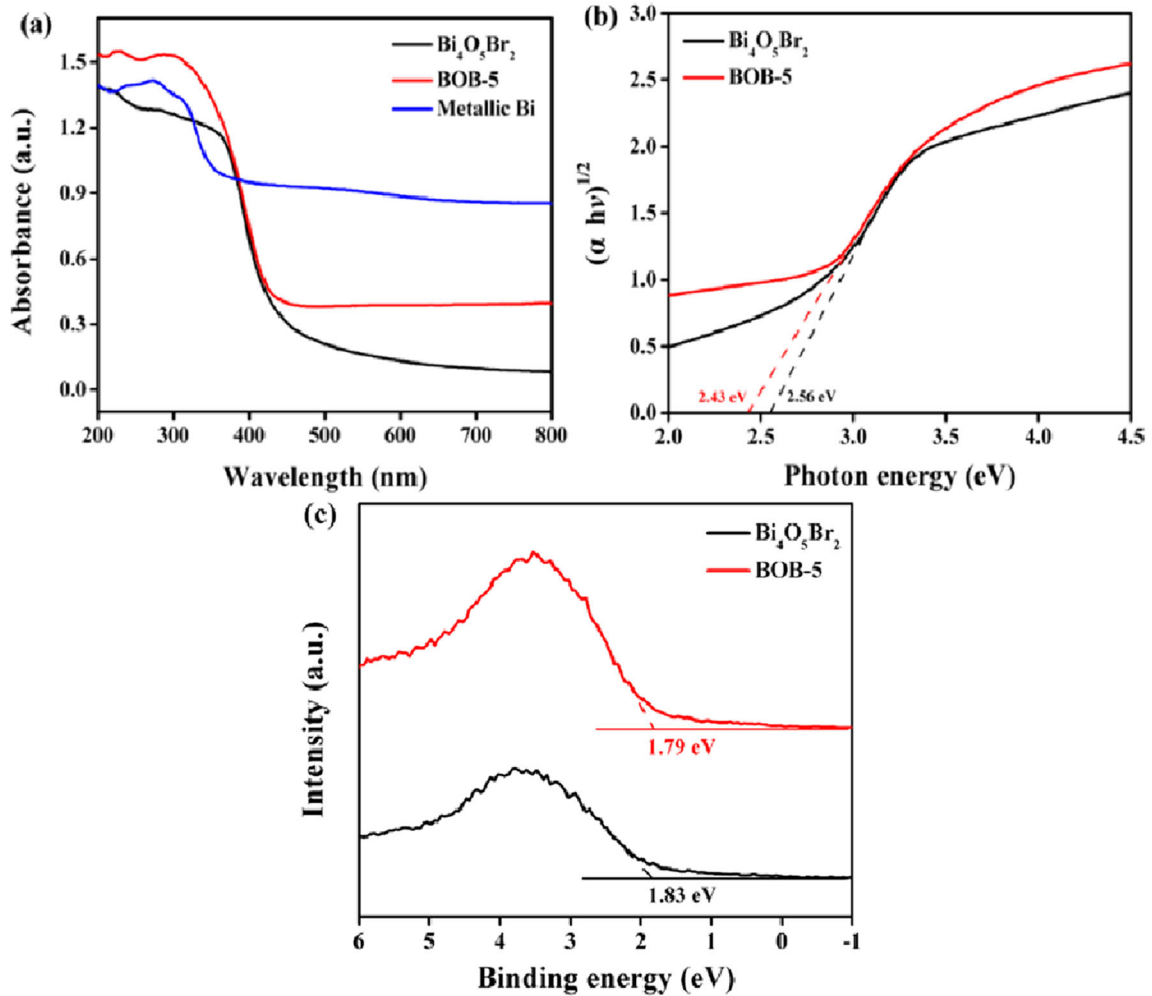


Fig. 10 UV-Vis diffuse reflectance spectra of $\text{Bi}_4\text{O}_5\text{Br}_2$ and BOB-5 samples (a); plot of $(\alpha h\nu)^2$ versus $h\nu$ for $\text{Bi}_4\text{O}_5\text{Br}_2$ and BOB-5 (b); VB-XPS spectra of $\text{Bi}_4\text{O}_5\text{Br}_2$ and BOB-5 (c)

degradation rate. The rate constants for the degradation of RhB and BPA by BOB-5 were 4.6 times and 13.1 times higher than those of the pure substances, respectively.

The reusability of photocatalysts is of great importance in industrial applications. Figure 8a is the degradation efficiency results for five cycle experiments. Catalyst stability and reusability can be verified. When RhB was degraded under the same conditions, the catalytic performance activity loss rate of BOB-5 sample was within 10% even after five cycles, with no obvious activity loss. Figure 8b is a comparison of the infrared spectra before and after the cycle experiment, and the infrared spectrum before and after the cycle experiment did not change significantly. It can be seen that the composite material BOB-5 has good stability and cyclability, and has the prospect of further participation in industrial applications.

3.5 Optical properties and energy band analysis

Fluorescence spectroscopy can analyze the separation rate of photogenerated charge carriers in catalysts. The lower the emission peak, the lower the electron–

hole recombination efficiency. As shown in Fig. 9a, BOB-2, BOB-5 and BOB-10 have similar peak shapes and all show the maximum emission peak at 330 nm compared with the pure substance $\text{Bi}_4\text{O}_5\text{Br}_2$. The peak intensities of a series of complexes are reduced relative to $\text{Bi}_4\text{O}_5\text{Br}_2$. The intensity of the peak is proportional to the recombination rate of photogenerated carriers [29]. Therefore, the peak intensity of BOB-5 is the lowest, the separation rate of photogenerated carriers is the highest, and the photocatalytic performance is the best. Figure 9b is the fluorescence decay curve of $\text{Bi}_4\text{O}_5\text{Br}_2$ and BOB-5. The long fluorescence lifetime is due to the rapid recombination of electrons and holes, while the shorter fluorescence lifetime indicates the rapid transfer of photogenerated charges [30, 31]. The known average fluorescence lifetime calculation formula is:

$$t_{\text{average}} = \frac{(A_1 t_1^2 + A_2 t_2^2)}{(A_1 t_1 + A_2 t_2)}$$

where t_1 and t_2 represent the fluorescence lifetime, and A_1 and A_2 represent the amplitude [32]. The average fluorescence lifetime of $\text{Bi}_4\text{O}_5\text{Br}_2$ is 0.41 ns, and the average lifetime of BOB-5 is 0.37 ns. Therefore, the short fluorescence lifetime of BOB-5 can indicate the rapid transfer of photogenerated electrons and the enhanced photocatalytic performance.

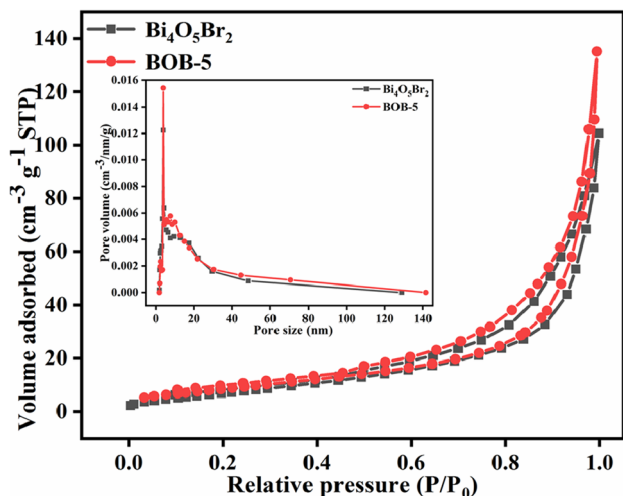


Fig. 11 N_2 adsorption–desorption isotherm of $\text{Bi}_4\text{O}_5\text{Br}_2$, BOB-5 and the corresponding pore size distribution curves (inset)

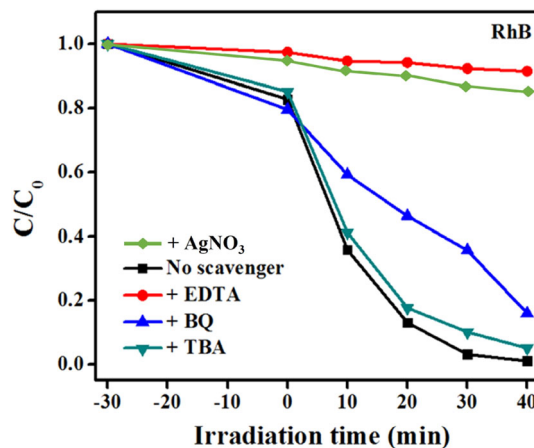


Fig. 12 Free radical capture experiment of BOB-5

Table 1 Specific surface areas, pore sizes, and pore volumes of $\text{Bi}_4\text{O}_5\text{Br}_2$ and BOB-5

Sample	Specific surface area/(m^2/g)	Pore volume/(cm^3/g)	Pore size/nm
$\text{Bi}_4\text{O}_5\text{Br}_2$	29.18	0.13	18.62
BOB-5	33.08	0.17	21.49

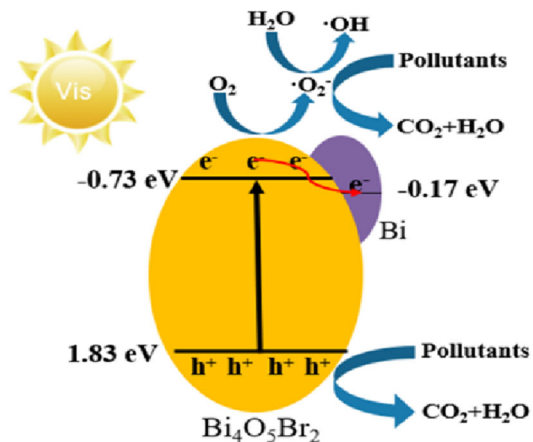


Fig. 13 Photocatalytic mechanism diagram of Bi/Bi₄O₅Br₂ complexes

The UV–Vis diffuse reflectance spectra of Bi₄O₅Br₂ and BOB-5 are shown in Fig. 10a, indicating that all samples absorb in the visible region. The absorption edges of Bi₄O₅Br₂ and BOB-5 samples are at 440 nm and 450 nm, respectively, and the absorption of the composites is slightly red-shifted. This indicates that the light absorption range of the composite is broadened after Bi deposition on Bi₄O₅Br₂, which may be one of the reasons for the improved photocatalytic performance. Figure 10b show that the forbidden band widths of Bi₄O₅Br₂ and BOB-5 samples are 2.56 eV and 2.43 eV, respectively. The narrowing of the band gap of the composite is beneficial to the separation of electron–hole pairs and enhances the photocatalytic performance [33, 34]. Figure 10c shows the VB-XPS spectra of Bi₄O₅Br₂ and BOB-5. It can be seen that the VB of the complex is reduced relative to the pure substance. This shows that the complexes are more likely to transfer electrons than pure substances.

3.6 Specific surface area and pore size analysis

BET tests the specific surface area of Bi₄O₅Br₂ and BOB-5 samples. Figure 11 is the nitrogen adsorption–desorption isotherm and pore size distribution (inset) of Bi₄O₅Br₂ and BOB-5. The results show that Bi₄O₅Br₂ and BOB-5 are both type IV isotherms, which belong to physical adsorption. The specific surface areas of Bi₄O₅Br₂ and BOB-5 are 29.18 and 33.08 m²/g, respectively, as can be seen from Table 1. BOB-5 has a larger specific surface area than Bi₄O₅Br₂. The

interpolated pore size distribution map also indicated the existence of mesoporous structure in Bi₄O₅Br₂ and BOB-5 samples. In general, the mesoporous structure and higher specific surface area can increase the surface active sites and provide an efficient transport path for reactants and products, thereby increasing the photocatalytic degradation activity [35]. Therefore, the increase in the specific surface area of BOB-5 may be one of the reasons for its enhanced photocatalytic activity.

3.7 Analysis of photocatalytic mechanism

The reaction mechanism in the photocatalytic degradation process was explored through radical trapping experiments. In the photocatalytic degradation of RhB by BOB-5, 0.372 g of EDTA, 0.02 g of p-benzoquinone (BQ), 48 μL of silver nitrate solution (AgNO₃) and 48 μL of tert-butyl (TBA) were added as h⁺ (hole), OH[−] (hydroxyl radical), e[−] (electron) and ·O₂[−] (superoxide radical) scavenger, respectively [36]. The experimental results are shown in Fig. 12. However, the degradation curve fluctuated greatly when BQ was added, which may be due to the adsorption of BQ. The presence of TBA and AgNO₃ resulted in no significant change in the final degradation rate of RhB. However, EDTA significantly inhibited the degradation of RhB, suggesting that h⁺ plays a major role in the catalytic process.

Based on the above characterization and analysis, we propose a possible photocatalytic mechanism in Fig. 13. After the catalyst is excited by light, e[−] transitions from VB to CB, and h⁺ remains on VB. The conduction band width of Bi₄O₅Br₂ can be calculated to be −0.73 eV from the known characterization, and the Fermi level of metallic bismuth is −0.17 eV [33]. Due to the high and low potential difference, photoexcited electrons can be transferred from Bi₄O₅Br₂ to metallic Bi. Semimetal Bi has the SPR effect and has the ability to attract electrons. Therefore, after the electrons are separated from the holes in the valence band, they are transferred to the semimetal Bi. This inhibits the recombination of photogenerated carriers and improves the photocatalytic performance. Under the action of ·O₂[−] and h⁺, the pollutants open the ring, and finally decompose into CO₂ and H₂O.

4 Conclusion

In conclusion, Bi/Bi₄O₅Br₂ composite photocatalysts with different loadings were prepared by in situ reduction method. The composites with a loading of 5% exhibited excellent photocatalytic performance compared to the Bi₄O₅Br₂. Compared with the pure substance, the morphology of this complex remains intact and the size is slightly larger. The enlarged photoresponse range and the reduced recombination rate of photogenerated carriers enhance the photocatalytic performance of the composites. The composite photocatalyst has good cycle stability and has industrial application prospects.

Acknowledgements

This work was supported by National Natural Science Foundation of China (No. 21171053) and the Natural Science Foundation of Hubei Province Education Committee, China (D20213102).

Author contributions

All authors contributed to this research work. The scheme design, material preparation, data collection and analysis were carried out by CL, ZZ, PC and YY. The first draft of the manuscript was written by ZX, and professor SY participated in the whole process of guidance. All authors have commented on previous manuscript versions. All authors read and approved the final manuscript.

Funding

This study was supported by National Natural Science Foundation of China, Grant No. 21171053, The Natural Science Foundation of Hubei Province Education Committee, China, Grant No. D20213102.

Data availability

The materials used and analyzed during the current study are available from the corresponding author on reasonable request.

Declarations

Competing interest The authors declare that they have no known competing financial interests or personal relationships that could have appeared to influence the work reported in this paper.

5. References

1. T. An, H. Yang, G. Li, W. Song, W.J. Cooper, X. Nie, Kinetics and mechanism of advanced oxidation processes (AOPs) in degradation of ciprofloxacin in water. *Appl. Catal. B* **94**, 288–294 (2010)
2. J. Kong, T. Yang, Z. Rui, H. Ji, Perovskite-based photocatalysts for organic contaminants removal: current status and future perspectives. *Catal. Today* **327**, 47–63 (2019)
3. Hu. Hao, Lv. Qin, F. Shiya, Li. Xiongjian, Y. Yun, Y. Shuijin, Solvothermal synthesis of polyoxometalate-modified UiO-66-NH₂ for enhanced removal of ciprofloxacin from aqueous solution. *J. Mater. Sci: Mater Electron*. **33**, 4184–4196 (2022)
4. P. Chen, Z. Zhang, S. Yang, Y. Yang, Synthesis of BiOCl/ZnMoO₄ heterojunction with oxygen vacancy for enhanced photocatalytic activity. *J. Mater. Sci: Mater Electron*. **32**, 23189–23205 (2021)
5. X. Jin, L. Ye, H. Xie, G. Chen, Bismuth-rich bismuth oxyhalides for environmental and energy photocatalysis. *Coord. Chem. Rev.* **349**, 84–101 (2017)
6. Lu. Ziyang, X. Zhao, Z. Zhu, Y. Yan, W. Shi, H. Dong, Z. Ma, N. Gao, Y. Wang, H. Huang, E. Recyclability, Stability, and selectivity of CdS/C@Fe₃O₄ nanoreactors for orientation photodegradation of ciprofloxacin. *Chem. Eur. J.* **21**, 18528–18533 (2015)
7. Xu. Zhang, P. Yang, Bo. Yang, Y. Bai, W. Liu, Qi. Wang, Synthesis of novel Bi/Bi₄O₅Br₂ via a UV light irradiation for decomposing the oil field pollutants. *Inorg. Chem. Commun.* **122**, 108297 (2020)
8. X. Mao, F. Xie, M. Li, Facile hydrolysis synthesis of novel Bi₄O₅Br₂ photocatalyst with enhanced visible light photocatalytic activity for the degradation of resorcinol. *Mater. Lett.* **166**, 296–299 (2016)
9. W. Zhang, X. Xiao, Wu. Qingfeng, Q. Fan, S. Chen, W. Yang, F. Zhang, Facile synthesis of novel Mn-doped Bi₄O₅Br₂ for enhanced photocatalytic NO removal activity. *J. Alloy. Compd.* **826**, 154204 (2020)
10. M. Ge, J. Cai, J. Icozzia, C. Cao, J. Huang, X. Zhang, J. Shen, S. Wang, S. Zhang, K. Zhang, Y. Lai, Z. Lin, A review of TiO₂ nanostructured catalysts for sustainable H₂ generation. *Int. J. Hydrogen Energy* **2**, 8418–8449 (2017)

11. He. Rongan, C. Shaowen, Yu. Jiaguo, Recent advances in morphology control and surface modification of Bi-based photocatalysts. *Acta Phys. -Chim. Sin.* **32**(12), 2841–2870 (2016)
12. S. Shafafi, A. Habibi-Yangjeh, S. Feizpoor, S. Ghosh, T. Maiyalagan, Carbon dots and Bi₄O₅Br₂ adhered on TiO₂ nanoparticles: impressively boosted photocatalytic efficiency for removal of pollutants under visible light. *Sep. Purif. Technol.* **250**, 117179 (2020)
13. F.A. Marzouqi, B.A. Farsi, A.T. Kuvarega, H.A.J. Al, S.M.Z. Lawati, A. Kindy, Y. Kim, R. Selvaraj, Controlled microwave-assisted synthesis of the 2D-BiOCl/2D-g-C₃N₄ heterostructure for the degradation of amine-based pharmaceuticals under solar light illumination. *ACS Omega* **4**, 4671–4678 (2019)
14. Z. Guan, X. Li, Wu. You, Z. Chen, X. Huang, D. Wang, Qi. Yang, J. Liu, S. Tian, X. Chen, H. Zhao, AgBr nanoparticles decorated 2D/2D GO/Bi₂WO₆ photocatalyst with enhanced photocatalytic performance for the removal of tetracycline hydrochloride. *Chem. Eng. J.* **410**, 128283 (2021)
15. F. Deng, Q. Zhang, L. Yang, X. Luo, A. Wang, S. Luo, D.D. Dionysiou, Visible-light-responsive graphene-functionalized Bi-bridge Z-scheme black BiOCl/Bi₂O₃ heterojunction with Oxygen vacancy and multiple charge transfer channels for efficient photocatalytic degradation of 2-nitrophenol and Industrial wastewater treatment. *Appl. Catal. B* **238**, 61–69 (2018)
16. L. Zeng, F. Zhe, Y. Wang, Q. Zhang, X. Zhao, Hu. Xin, Wu. Ying, Y. He, Preparation of interstitial carbon doped BiOI for enhanced performance in photocatalytic nitrogen fixation and methyl orange degradation. *J. Colloid Interface Sci.* **539**, 563–574 (2019)
17. Z. Zhao, W. Zhang, Y. Sun, Yu. Jiayan, Y. Zhang, H. Wang, F. Dong, Wu. Zhongbiao, Bi Cocatalyst/Bi₂MoO₆ microspheres nano hybrid with SPR-promoted visible-light photocatalysis. *J. Phys. Chem. C.* **120**, 11889–11898 (2016)
18. M. Liang, Z. Yang, Y. Yang, Y. Mei, H. Zhou, S. Yang, One-step introduction of metallic Bi and non-metallic C in Bi₂WO₆ with enhanced photocatalytic activity. *J. Mater. Sci: Mater Electron.* **30**, 1310–1321 (2019)
19. X. Jin, C. Lv, X. Zhou, H. Xie, S. Sun, Y. Liu, Q. Meng, G. Chen, A Bismuth rich hollow Bi₄O₅Br₂ photocatalyst enables dramatic CO₂ reduction activity. *Nano Energy* **64**, 103955 (2019)
20. Di. Liu, W. Yao, J. Wang, Y. Liu, Mo. Zhang, Y. Zhu, Enhanced visible light photocatalytic performance of a novel heterostructured Bi₄O₅Br₂/Bi₂4O₃1Br₁₀/Bi₂SiO₅ photocatalyst. *Appl. Catal. B* **172–173**, 100–107 (2015)
21. Y. Bai, P. Yanga, Li. Wang, Bo. Yang, H. Xie, Y. Zhou, L. Ye, Ultrathin Bi₄O₅Br₂ nanosheets for selective photocatalytic CO₂ conversion into CO. *Chem. Eng. J.* **360**, 473–482 (2019)
22. S. Wang, X. Hai, X. Ding, K. Chang, Y. Xiang, X. Meng, Z. Yang, H. Chen, J. Ye, Light-Switchable oxygen vacancies in ultrafine Bi₅O₇Br nanotubes for boosting solar-driven nitrogen fixation in pure water. *Adv. Mater.* **29**, 1701774 (2017)
23. J. Li, W. Zhang, M. Ran, Y. Sun, H. Huang, F. Dong, Synergistic integration of Bi metal and phosphate defects on hexagonal and monoclinic BiPO₄: enhanced photocatalysis and reaction mechanism. *Appl. Catal. B* **243**, 313–321 (2019)
24. F. Yi, J. Ma, C. Lin, L. Wang, H. Zhang, Y. Qian, K. Zhang, Insights into the enhanced adsorption/photocatalysis mechanism of a Bi₄O₅Br₂/g-C₃N₄ nanosheet. *J. Alloy. Compd.* **821**, 153557 (2020)
25. X. Li, B. Kang, F. Dong, Z. Zhang, L. Xudong Luo, J.H. Han, Z. Fang, Z. Chen, X. Jilin, B. Peng, Z. Wang, Enhanced photocatalytic degradation and H₂/H₂O₂ production performance of S-pCN/WO S-scheme heterojunction with appropriate surface oxygen vacancies. *Nano Energy* **81**, 105671 (2021)
26. M. Ji, J. Di, Y. Ge, J. Xia, H. Li, 2D–2D stacking of graphene-like G-C₃N₄/ultrathin Bi₄O₅Br₂ with matched energy band structure towards antibiotic removal. *Appl. Surf. Sci.* **413**, 372–380 (2017)
27. J. Liu, R. Li, Zu. Xiang, X. Zhang, Y. Wang, Y. Wang, C. Fan, Photocatalytic conversion of nitrogen to ammonia with water on triphase interfaces of hydrophilic-hydrophobic composite Bi₄O₅Br₂/ZIF-8. *Chem. Eng. J.* **371**, 796–803 (2019)
28. G. Zhu, S. Li, J. Gao, F. Zhang, C. Liu, Q. Wang, M. Hojamberdiev, Constructing a 2D/2D Bi₂O₂CO₃/Bi₄O₅Br₂ heterostructure as a direct Z-scheme photocatalyst with enhanced photocatalytic activity for NO_x removal. *Appl. Surf. Sci.* **493**, 913–925 (2019)
29. X. Wang, C. Liow, A. Bisht, X. Liu, T.C. Sum, X. Chen, S. Li, Engineering interfacial photo-induced charge transfer based on nanobamboo array architecture for efficient solar-to-chemical energy conversion. *Adv. Mater.* **27**, 2207–2214 (2015)
30. J. Zhou, R. Wang, X. Liu, F. Peng, C. Li, F. Teng, Y. Yuan, In situ growth of CdS nanoparticles on UiO-66 metal-organic framework octahedrons for enhanced photocatalytic hydrogen production under visible light irradiation. *Appl. Surf. Sci.* **346**, 278–283 (2015)
31. Y. Zhang, Y. Tang, X. Liu, Z. Dong, H.H. Hng, Z. Chen, T.C. Sum, X. Chen, Three-dimensional CdS-titanate composite nanomaterials for enhanced visible-light-driven hydrogen evolution. *Smal.* **9**, 996–1002 (2012)

32. Y. He, X. Jin, W. Li, S. Yang, B. Lv, Preparation and photocatalytic properties of $\text{Bi}_2\text{WO}_6/\text{UiO}-66$ composites. *Chin. J. Inorg. Chem.* **35**(6), 996–1004 (2019)
33. X. Lian, W. Xue, S. Dong, E. Liu, H. Li, Xu. Kangzhen, Construction of S-scheme $\text{Bi}_2\text{WO}_6/\text{g}-\text{C}_3\text{N}_4$ heterostructure nanosheets with enhanced visible-light photocatalytic degradation for ammonium dinitramide. *J. Hazard. Mater.* **412**, 125217 (2021)
34. C. Zou, M. Liang, Z. Yang, X. Zhou, Y. Yang, S. Yang, Flower-like $\text{Bi}_2\text{SiO}_5/\text{Bi}_4\text{MoO}_9$ heterostructures for enhanced photocatalytic degradation of ciprofloxacin. *NANO* **31**, 345604 (2020)
35. Y. Huang, S. Kang, Y. Yang, H. Qin, Z. Ni, S. Yang, Xi. Li, Facile synthesis of $\text{Bi}/\text{Bi}_2\text{WO}_6$ nanocomposite with enhanced photocatalytic activity under visible light. *Appl. Catal. B* **196**, 89–99 (2016)
36. H. Shi, W. Wang, L. Zhang, Z. Tang, J. Fan, Enhancement of photocatalytic disinfection performance of the $\text{Bi}_4\text{O}_5\text{Br}_2$ with the modification of silver quantum dots. *J. Environ. Chem. Eng.* **9**, 105867 (2021)

Publisher's Note Springer Nature remains neutral with regard to jurisdictional claims in published maps and institutional affiliations.

Springer Nature or its licensor (e.g. a society or other partner) holds exclusive rights to this article under a publishing agreement with the author(s) or other rightsholder(s); author self-archiving of the accepted manuscript version of this article is solely governed by the terms of such publishing agreement and applicable law.